ChemPubSoc Europe

DOI: 10.1002/ejic.201600199

EurJIC European Journal of Inorganic Chemistry

Full Paper

Magnetic Cyanoferrates

CLUSTER ISSUE

Structure-Property Relationships in Tricyanoferrate(III) Building Blocks and Trinuclear Cyanide-Bridged Complexes

Yuanzhu Zhang,[a] Uma P. Malik,[a] Benjamin Quiggins,[a] Hung Nguyen,[a] Christopher C. Beedle,[b] Alexey E. Kovalev,[b] Rodolphe Clérac,[c,d] Stephen Hill,[b,e] Benjamin J. Bythell,[a] and Stephen M. Holmes*[a,f]

Abstract: The preparation, structures, and magnetic properties of two tricyanoferrates, $[NEt_4]_2[(Tp^{*Me})Fe^{II}(CN)_3]\cdot MeCN$ (**1**) and $[NEt_4][(Tp^{*Me})Fe^{III}(CN)_3]\cdot H_2O$ (**2**), and three trinuclear derivatives, $\{[(Tp^{*Me})Fe^{III}(CN)_3]_2[Ni^{II}(L)_2]\}\cdot n(solvent)$ (L = bpy, **3**; tren, **4**; DETA, **5**) are described. Magnetic measurements show that **2** is an $S = {}^1/_2$ complex [$g = 2.65(1)$], while **3**–**5** display $S_T = 2$ spin ground states, owing to cyanide-mediated ferromagnetic exchange between Fe^{III}_{LS} ($S = {}^1/_2$) and Ni^{II} ($S = 1$) ions. The χT vs. T data for **3**–**5** were modelled using an isotropic Heisenberg model and give J/k_B and g_{avg} values of +11.1(1) K and 2.48(1) for **3**, 9.1(1) K and 2.6(1) for **4**, and +11.2(1) K and 2.41(5) for **5** (with $zJ' = -0.28$ K). High-field/frequency EPR data indicates significant g-anisotropy in **2** ($g_z = 3.6$, $g_y = 2.2$, $g_x = 2.0$) and $[NEt_4][(Tp^*)Fe^{III}(CN)_3]\cdot H_2O$ (**6**) ($g_z = 3.5$, $g_y = 2.0$, $g_x = 1.3$), while **5** shows $D = -2.09$ cm^{-1}, $E = 0.08$ cm^{-1}, and $B_4{}^0 = -2.3 \times 10^{-3}$ cm^{-1} with $g_z = 2.4$ and $g_x = g_y = 1.95$. Despite significant magnetic anisotropy in **3**–**5**, frequency-dependent behavior is only seen for **5** above 1.8 K, suggesting that rapid quantum tunnelling of the magnetization is operative.

Introduction

Single-molecule magnets (SMMs) have received considerable attention over the past two decades as their study lies at the interfaces of chemistry, materials, and physics disciplines.[1–13] Among these are polynuclear complexes derived from cyanometalate anions, whose magnetic anisotropies arise from unquenched orbital angular momentum, a necessary criterion for the creation of an appreciable spin-reversal energy barrier.[10–53] Of known cyanide-based SMMs those containing $[(Tp^R)Fe^{III}(CN)_3]^-$ building blocks, where Tp^R is a tridentate poly(pyrazolyl)borate, have seen extensive use in construction of polynuclear complexes that exhibit slow magnetic relaxation.[12–16,19–21,28–47,50–53]

Pyrazolylborates are an attractive class of *fac*-coordinate ancillary ligands for constructing structurally related families of polynuclear complexes.[12–16,19–21,28–47,50–54] Through selective chemical substitution the electronic, steric, and solubility properties of the molecular precursors (building blocks) may be systematically altered with atom-economical precision and efficiency. These tunable tridentate capping ligands are known to stabilize a variety of metal centers and multiple oxidation states, and their cyanido complexes can be controllably aggregated to form discrete clusters under a range of synthetic conditions. By careful control of stoichiometry and ligand steric demand the numbers and spatial orientations of formed M(μ-CN)M′ units may be systematically altered and afford materials with tunable magnetic and optical properties, namely those that display slow magnetic relaxation, e.g. single-molecule magnets,[12–16,20,21,28–45] single-chain magnets,[19,46–53] spin-crossover,[67–70] and photoresponsive[55–67] behavior.

In polynuclear complexes containing (polypyrazolylborato)tricyanoferrate(III) ions, $[(Tp^R)Fe^{III}_{LS}(CN)_3]^-$ ($S = {}^1/_2$), the doubly degenerate (^2E) spin ground states provide efficient first-order orbital contributions that lead to appreciable magnetic anisotropy ($2.3 \le g \le 2.9$).[12,14–16,19–21,28–47,53] Through deliberate self-assembly of these building blocks their single-ion anisotropy properties may be exploited to create polynuclear derivatives that display slow magnetic-relaxation dynamics. The most commonly studied analogues contain cyanide-bridged paramagnetic iron(III) and nickel(II) ions, whose spatial arrangement of $Fe^{III}_{LS}(\mu\text{-}CN)Ni^{II}$ units are highly dependent on the steric demand of the Tp^R ligands; $Fe^{III}_{LS}(\mu\text{-}CN)Ni^{II}$ fragment linearity is often strongly correlated with efficient ferromagnetic superexchange.

We were the first to describe relationships linking SMM energy-barrier heights and orientations of their putative anisotropy tensors (pseudo-C_3 rotation axes, B···Fe) in polynuclear

[a] *Department of Chemistry & Biochemistry, University of Missouri – St. Louis, St. Louis, Missouri 63121, USA*
E-mail: holmesst@umsl.edu
www.umsl.edu/chemistry/Faculty/holmes.html
[b] *National High Magnetic Field Laboratory, Tallahassee, Florida 32306, USA*
[c] *CNRS, CRPP, UPR 8641, 33600 Pessac, France*
[d] *Univ. Bordeaux, CRPP, UPR 8641, 33600 Pessac, France*
[e] *Department of Physics, Florida State University, Tallahassee, Florida 32310, USA*
[f] *Center for Nanoscience, University of Missouri-St. Louis, St. Louis, Missouri 63121, USA*

Supporting information for this article is available on the WWW under http://dx.doi.org/10.1002/ejic.201600199.

Fe^{III}/Ni^{II} clusters. We discovered that collinear arrangements generally lead to higher spin-reversal barriers and slower magnetic relaxation than those containing bent Fe^{III}_{LS}(μ-CN)Ni^{II} bridges and/or misaligned B···Fe units.[12,14–17,51–53,68–72] Both features may be controlled by steric demand of the pyrazolylborate ligands in the $[(Tp^{R})Fe^{III}_{LS}(CN)_3]^-$ building blocks. For example, in octanuclear $\{Fe^{III}_4Ni^{II}_4\}$, the presence of sterically demanding Tp*Me {tris[3,4,5-trimethyl(pyrazol-1-yl)borate]} ligands afford a low-symmetry C_2-symmetric complex,[34] while – identical synthetic conditions – smaller tetra(pyrazol-1-yl)borates [pzTp] give higher-symmetry molecular boxes. The nearly linear Fe^{III}_{LS}(μ-CN)Ni^{II} units present in both analogues lead to efficient ferromagnetic interactions (J/k_B = 9.0 K), but a threefold difference in their experimental SMM energy barriers is found (Δ/k_B ≈ 33 vs. 12 K),[31,32,34] suggesting that spatial arrangements of their single-ion anisotropy tensors are strongly correlated with molecular structure and quantum tunnelling of the magnetization; we note that the B···Fe axes are parallel in the low-symmetry octanuclear analogue, while those in the cubic box are directed towards the body center.

In a continuing effort to understand the origins of single-ion anisotropy and how it leads to the creation of energy barriers to magnetic relaxation in polynuclear complexes, we turned our attention towards cyanide-bridged $\{Fe^{III}_2Ni^{II}\}$ trinuclear analogues, as only three SMMs have been reported to date.[12,15,28,32,40,41,45,58] This system was deliberately chosen as ligand–ligand steric interactions easily translate into tunable Fe^{III}(μ-CN)Ni^{II} distortions within a common structural archetype. We reasoned that controlling the relative orientations of their single-ion anisotropy tensors (e.g. Fe···B vectors) would ultimately lead to higher SMM energy barriers. In this contribution, we report on the structures, magnetic, and spectroscopic properties of two tricyanoferrate complexes and three structurally related trinuclear $\{Fe^{III}_2Ni^{II}\}$ derivatives.

Results and Discussion

Two tricyanoferrate complexes may be prepared by modifications to previously described synthetic methods.[30,34] Sequential treatment of $Fe(OAc)_2$ with KTp*Me, followed by excess $[NEt_4]CN$ in acetonitrile gives $[NEt_4]_2[(Tp^{*Me})Fe^{II}(CN)_3]$·MeCN (**1**) as a divalent complex (Supporting Information). A second trivalent analogue, $[NEt_4][(Tp^{*Me})Fe^{III}(CN)_3]$·$H_2O$ (**2**), is obtained upon hydrogen peroxide addition to CH_2Cl_2/*i*PrOH solutions of **1**. The solid-state infrared spectra of **1** and **2** display high energy and intense ν_{BH} [2507 and 2544 cm^{-1}] and ν_{CN} [2044 and 2119 cm^{-1}] stretching absorptions, which indicate that coordinated Tp*Me and cyanide ligands are present.[34,35,74,75] The ν_{CN} stretches seen for **1** and **2** are shifted to higher energies in comparison to that seen for $[NEt_4]CN$ (2056 cm^{-1})[74] and are in ranges expected for cyanides coordinated to di- (2044 cm^{-1}) and trivalent (2119 cm^{-1}) iron centers, respectively.[12,15,16,19–21,28–53,55–66,68,71,72] Subsequent treatment of **2** with $Ni(ClO_4)_2$·$6H_2O$ or $NiCl_2$·$6H_2O$, followed by either 2,2′-bipyridine (bpy), tren [tris(2-aminoethyl)amine], or DETA (diethylenetriamine) affords trinuclear complexes of $\{[(Tp^{*Me})Fe^{III}(CN)_3]_2[Ni^{II}(bpy)_2]\}$·$3H_2O$·4MeOH (**3**), $\{[(Tp^{*Me})Fe^{III}(CN)_3]_2[Ni^{II}(tren)]\}$·$2H_2O$·3MeOH (**4**), and $\{[(Tp^{*Me})Fe^{III}(CN)_3]_2[Ni^{II}(DETA)(OH_2)]\}$·$6H_2O$·MeCN (**5**) stoichiometry, respectively.

Complexes **3**–**5** display two cyanide stretches in their infrared spectra signalling the presence of bridging and terminal cyanides.[12,15,21,28–47,75,76] The highest-energy ν_{CN} absorptions (2159, 2153, and 2154 cm^{-1}) correspond to bridging cyanides, while the lower-energy ones (2121, 2119, and 2122 cm^{-1}) belong to terminal cyanides, as they closely resemble those seen in the infrared spectrum of **2**. Consistent with this assumption the ν_{BH} stretches in **3**–**5** (2533, 2536, and 2529 cm^{-1}) are also different than those of **2**, verifying that the electronic environments of the iron centers have been altered. The infrared spectrum of **5** also exhibits additional strong- and medium-intensity absorptions (ν_{OH}, 3505; δ_{HOH}, 1625 cm^{-1}) suggesting that hydrogen-bonded lattice water and coordinated aqua ligands are also present.[12,21,30–45,75,76]

Tricyanometalate complexes **1** and **2** crystallize in the orthorhombic ($Pca2_1$) and monoclinic ($P2_1/n$) space groups, respectively (Table 1 and Figure 1).[77] Both adopt idealized C_{3v}-symmetric *fac*-FeN_3C_3 coordination geometries owing to the pres-

Table 1. Crystallographic data for $[NEt_4]_2[(Tp^{*Me})Fe^{II}(CN)_3]$·MeCN (**1**), $[NEt_4][(Tp^{*Me})Fe^{III}(CN)_3]$·$H_2O$ (**2**), $\{[(Tp^{*Me})Fe(CN)_3]_2[Ni(bpy)_2]\}$·$3H_2O$·4MeOH (**3**), $\{[(Tp^{*Me})Fe^{III}(CN)_3]_2[Ni^{II}(tren)_2]\}$·$2H_2O$·3MeOH (**4**), and $\{[(Tp^{*Me})Fe^{III}(CN)_3]_2[Ni^{II}(DETA)(OH_2)]\}$·$6H_2O$·MeCN (**5**).

	1	2	3	4	5
Empirical formula	$C_{39}H_{70}BFeN_{12}$	$C_{21}H_{28}BFeN_{10}O$	$C_{66}H_{94}B_2Fe_2N_{22}NiO_7$	$C_{51}H_{84}B_2Fe_2N_{22}NiO_5$	$C_{48}H_{86}N_{22}B_2Fe_2NiO_7$
λ [Å]	0.71073	0.71073	0.71073	0.071073	0.71073
T [K]	100(2)	100(2)	100(2)	100(2)	100(2)
Crystal system	orthorhombic	monoclinic	orthorhombic	triclinic	triclinic
Space group	$Pca2_1$	$P2_1/n$	$Fdd2$	$P\bar{1}$	$P\bar{1}$
a [Å]	19.676(1)	9.9051(6)	29.766(2)	15.0913(7)	10.8033(4)
b [Å]	11.5187(8)	16.122(1)	60.876(5)	15.7035(7)	14.2267(6)
c [Å]	18.651(1)	20.399(1)	18.185(2)	17.419(1)	21.6791(8)
α [°]	90	90	90	112.162(3)	103.403(2)
β [°]	90	93.661(2)	90	102.829(3)	94.549(2)
γ [°]	90	90	90	105.691(2)	103.373(2)
V [Å^3]	4227.3(5)	3250.8(4)	32951(5)	3428.9(3)	3122.1(2)
Z	4	4	16	2	2
$\varrho_{calcd.}$ [mg m^{-3}]	1.216	1.270	1.209	1.237	1.357
μ [mm^{-1}]	0.400	0.503	0.633	0.7545	0.822
R_1[a]	0.0375	0.0447	0.0828	0.0764	0.0638
wR_2[a]	0.1049	0.1414	0.2200	0.2011	0.1818

[a] $I \geq 2\sigma(I)$: $R_1 = \Sigma||F_o| - |F_c||/\Sigma|F_o|$, $wR_2 = \{\Sigma[w(F_o^2 - F_c^2)^2]/\Sigma[w(F_o^2)^2]\}^{1/2}$.

ence of sterically demanding tridentate Tp*Me [Tp*Me = κ3-hydridotris(3,4,5-trimethylpyrazol-1-yl)borate] ligands (Figure 1). The average Fe–C [1.903(2) and 1.921(2) Å] and Fe–N [2.052(1) and 2.005(1) Å] bond lengths suggest that π-back bonding plays a role in their structures (Table 2).[12,30,32,72,76,77] For example, if electrostatic Fe–C and Fe–N interactions dominate, then short bonds would be expected for the trivalent **2**, while comparatively longer ones should be seen for divalent **1**.[12,15,16,19–21,28–45] While comparable Fe–N distances are seen for both complexes, the shortest Fe–C bonds are found in **1** suggesting that efficient π-back bonding into the π^*_{CN} orbital is operative.[12,32,75] Consistent with this assumption the infrared spectrum of **1** exhibits a lower ν_{CN} stretching energy in comparison to **2**.

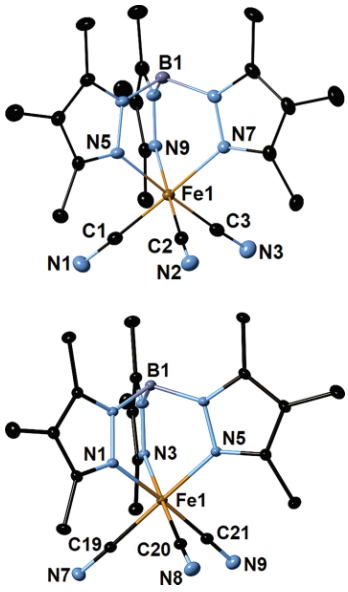

Figure 1. X-ray structures of (top) **1** and (bottom) **2**. All cations, lattice solvent, and hydrogen atoms are omitted for clarity, and thermal ellipsoids are at the 50 % level.

Table 2. Selected bond lengths [Å] and angles [°] for $[NEt_4]_2[(Tp^{*Me})Fe^{II}(CN)_3]$·MeCN (**1**) and $[NEt_4][(Tp^{*Me})Fe^{III}(CN)_3]$·$H_2O$ (**2**).

1		**2**	
Fe1–C1	1.909(2)	Fe1–C19	1.921(2)
Fe1–C2	1.899(2)	Fe1–C20	1.920(2)
Fe1–C3	1.901(2)	Fe1–C21	1.923(2)
Fe1–N5	2.065(1)	Fe1–N1	2.002(1)
Fe1–N7	2.047(1)	Fe1–N3	2.006(1)
Fe1–N9	2.044(1)	Fe1–N95	2.007(1)
C1–N1	1.162(2)	C19–N7	1.149(2)
C2–N2	1.164(2)	C20–N8	1.153(2)
C3–N3	1.168(2)	C21–N9	1.154(2)
C1–Fe1–C2	89.86(7)	C19–Fe1–C20	89.34(7)
C1–Fe1–C3	92.34(7)	C19–Fe1–C21	86.90(7)
C2–Fe1–C3	91.20(7)	C20–Fe1–C21	87.45(7)
C1–Fe1–N5	89.64(6)	C19–Fe1–N1	90.37(6)
C1–Fe1–N7	177.80(6)	C19–Fe1–N3	91.36(6)
C1–Fe1–N9	91.88(6)	C19–Fe1–N5	179.01(6)
N5–Fe1–N7	88.47(6)	N1–Fe1–N3	89.24(5)
N5–Fe1–N9	87.20(6)	N1–Fe1–N5	89.82(5)
N7–Fe1–N9	88.47(6)	N3–Fe1–N5	89.20(5)

Structures of **1** and **2** also display bond angles that are reflective of their ionic radii differences. The C–Fe1–C and N–Fe1–N angles vary slightly between 89.86(7) and 91.20(7)° and 87.20(6) and 88.47(6)° in **1** and are in the range seen for many $[(Tp^R)Fe^n(CN)_3]^{4-n}$ anions (Table 2).[12,30,32,76,77] In comparison, the C–Fe–C [86.90(7)–89.34(7)°] angles in **2** are more acute, while the N–Fe–N angles [89.20(5)–89.82(5)°] are slightly larger, suggesting that the trivalent ions are somewhat congested in comparison. The mean plane Fe•••$[N_{pz}]_3$ pyrazolylate contacts [1.224(2) and 1.169(5) Å], where $[N_{pz}]_3$ is defined as the distance between Fe^{III} to the centroid of the coordinated nitrogen atoms {N5–N7–N9} and {N1–N3–N5}, are also shorter in **2**, being consistent with a smaller ionic radius and higher charge density.[12,30,32,76,77] Along the crystallographic *a*-direction additional hydrogen-bonding interactions between lattice water and terminal cyanides are also found in structures of **2** (Figure S1) in addition to close intermolecular Tp*Me methyl–methyl contacts [ca. 4.233(3) Å].

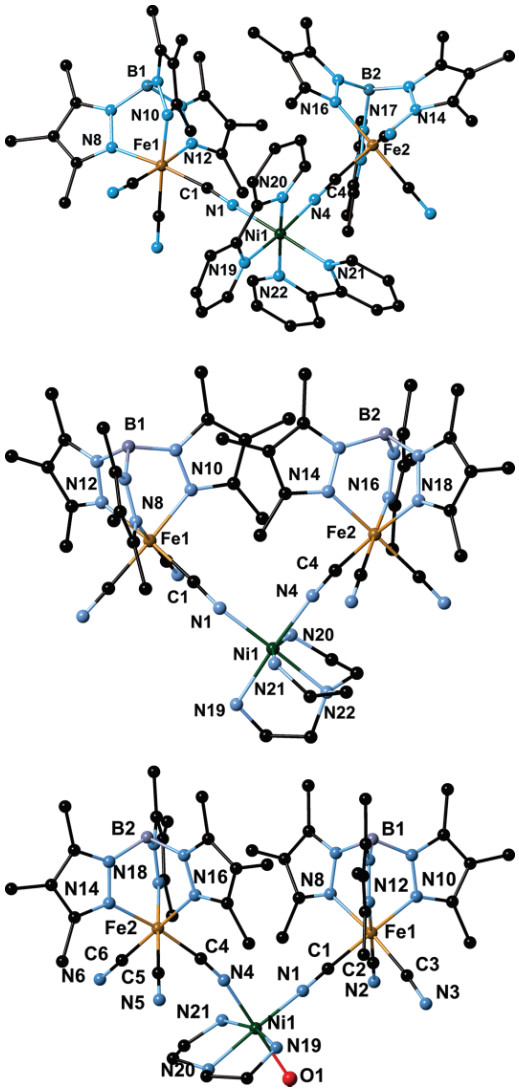

Figure 2. X-ray structures of **3** (top), **4** (middle), and **5** (bottom). All lattice solvent and hydrogen atoms are omitted for clarity.

Complexes **3** and **4** crystallize in the orthorhombic (*Fdd*2) and triclinic ($P\bar{1}$) space groups, respectively (Table 1).[77] Compounds **3** and **4** are structurally related neutral trinuclear complexes composed of two crystallographically independent $[(Tp^{*Me})Fe^{III}(CN)_2(\mu\text{-}CN)]^-$ anions linked to a central $[cis\text{-}Ni^{II}(L)(\mu\text{-}NC)_2]^{2+}$ (L = bpy, n = 2, **3**; tren, n = 1, **4**) fragment through cyanide bridges, leaving two terminal cyanides per Fe^{III} center (Figure 2, top and middle). The average Fe1–C [1.907(8) and 1.921(6) Å], Fe2–C [1.911(9) and 1.922(6) Å], and Ni1–N [2.059(7) and 2.094(5) Å] bonds in **4** are slightly longer than those in **3**, which may be related to the σ-donor ability of the more basic tren ligand (Table 3). Within the Fe1–C1–N1–Ni1 fragments the Fe1–C1–N1 and Ni1–N1–C1 angles [173.1(7) and 174.3(7)°] in **3** are comparable, while those in **4** are markedly different [173.6(5) and 165.9(5)°], suggesting that severe steric repulsion is operative in the latter complex. Intramolecular Fe1···Ni1 [ca. 5.090(8) and 5.10(1) Å] and Fe···Fe [ca. 7.292(8) and 7.361(8) Å] contacts are seen, while distant intermolecular Fe···Ni and Ni···Ni contacts of 9.426(7) and 8.876(7) Å are found for **3** and **4**, respectively; additional intercomplex ligand–ligand contacts are also present: 3.640(7) and 6.433(8) Å [Tp^{*Me}···Tp^{*Me} and bpy···bpy] and 3.500(8) and 3.995(7) Å [Tp^{*Me}···tren and Tp^{*Me}···Tp^{*Me}] for **3** and **4**, respectively (Table 3).

Crystals of **5** are found in the triclinic $P\bar{1}$ space group (Table 1).[76,77] The bent trinuclear $\{[Fe^{III}(\mu\text{-}CN)]_2Ni^{II}\}$ complex consists of crystallographically independent iron centers that are linked to a central $[cis\text{-}Ni^{II}(DETA)(OH_2)(\mu\text{-}NC)_2]^{2+}$ unit through bridging cyanides (Figure 2, bottom). The terminal cyanide Fe–C bonds [1.926(3) Å avg.] range between 1.917(3) and 1.934(3) Å [Fe2–C6 and Fe2–C5], while the bridging ones [Fe1–C1, 1.923(3) Å; Fe2–C4, 1.919(3) Å] adopt values seen in a variety of Fe^{III}/Ni^{II} complexes.[12,21,28–45,71] Within the Fe1–C1–N1–Ni1 fragment the Fe1–CN and Ni1–NC angles are nearly linear [178.4(3)° and 176.3(3)°], while those in the Fe2–C4–N4–Ni1 unit are more acute [173.1(3)° and 167.6(3)°], suggesting that significant steric congestion is present (Table 3).

In structures of **5**, the central $[cis\text{-}Ni^{II}(DETA)(OH_2)(\mu\text{-}NC)_2]$ fragment contains a tridentate *mer*-DETA ligand, two *cis*-cyanides, and a coordinated aqua ligand (Figure 2, bottom) that leads to a distorted six-coordinate NiN_5O environment. The Ni1–$N_{cyanide}$ bonds [2.030(3) and 2.079(3) Å] are slightly shorter than either of the Ni–N_{DETA}[2.084(3), 2.095(3), and 2.119(3) Å] or Ni1–O1 [2.145(2) Å] distances, while the cyanide C1–N1–Ni1 and C4–N4–Ni1 angles are markedly different [176.3(1) and 167.3(1)°] (Table 3). The *cis*-N–Ni–N(O) angles range between 82.0(1) [N20–Ni1–N21] and 99.2(1)° [N1–Ni1–N19] and participate in extensive hydrogen-bonding interactions between coordinated DETA, aqua ligands, and lattice water along the crystallographic *a*-direction (Figure S2). Short intermolecular O···$N_{cyanide}$ [2.752(4) Å], O···N_{DETA} [3.021(3) Å], and O···O [2.773(3)–2.994(3) Å] contacts are also found, while longer intramolecular Fe···Ni and Fe1···Fe2 [ca. 5.10(1) and 7.88(1) Å] and intermolecular Fe···Ni contacts of ca. 7.11(1) Å are found, respectively (Table 3). Thermogravimetric analysis (TGA) data confirm the presence of lattice water and that the anhydrous compounds remain stable up to ca. 200 °C (Figure S3).

The temperature dependence of the χT product at 1000 Oe confirms that **1** and **2** contain di- and trivalent iron centers,

Table 3. Selected bond lengths [Å] and angles [°] for $\{[(Tp^{*Me})Fe(CN)_3]_2[Ni(bpy)_2]\}\cdot 3H_2O\cdot 4MeOH$ (**3**), $\{[(Tp^{*Me})Fe^{III}(CN)_3]_2[Ni^{II}(tren)_2]\}\cdot 2H_2O\cdot 3MeOH$ (**4**), and $\{[(Tp^{*Me})Fe^{III}(CN)_3]_2[Ni^{II}(DETA)(OH_2)]\}\cdot 6H_2O\cdot MeCN$ (**5**).

3				**4**				**5**			
Fe1–C1	1.914(8)	C1–Fe1–C2	88.3(4)	Fe1–C1	1.910(6)	C1–Fe1–C2	86.7(2)	Fe1–C1	1.923(3)	C1–Fe1–C2	88.4(1)
Fe1–C2	1.898(9)	C1–Fe1–C3	81.5(3)	Fe1–C2	1.932(6)	C1–Fe1–C3	82.0(3)	Fe1–C2	1.925(3)	C1–Fe1–C3	84.7(1)
Fe1–C3	1.910(7)	C2–Fe1–C3	90.1(3)	Fe1–C3	1.921(6)	C2–Fe1–C3	90.1(3)	Fe1–C3	1.927(3)	C2–Fe1–C3	84.2(1)
Fe1–N8	1.981(6)	C1–Fe1–N8	94.2(3)	Fe1–N8	1.991(5)	C1–Fe1–N8	94.3(2)	Fe1–N8	2.014(3)	C1–Fe1–N8	91.0(1)
Fe1–N10	2.018(6)	C1–Fe1–N10	174.2(3)	Fe1–N10	1.998(5)	C1–Fe1–N10	94.7(2)	Fe1–N10	1.989(2)	C1–Fe1–N10	179.2(1)
Fe1–N12	1.983(6)	C1–Fe1–N12	92.9(3)	Fe1–N12	2.016(5)	C1–Fe1–N12	173.1(2)	Fe1–N12	1.991(2)	C1–Fe1–N12	91.1(1)
C1–N1	1.16(1)	Fe1–C1–N1	173.1(7)	C1–N1	1.153(7)	Fe1–C1–N1	173.6(5)	C1–N1	1.149(4)	Fe1–C1–N1	89.8(1)
C3–N3	1.15(1)	Fe1–C2–N2	176.4(8)	C3–N3	1.150(8)	Fe1–C2–N2	177.9(6)	C3–N3	1.153(4)	Fe1–C2–N2	90.0(1)
Fe2–C4	1.902(9)	Fe1–C3–N3	175.9(7)	Fe2–C4	1.899(6)	Fe1–C3–N3	176.6(6)	Fe2–C4	1.919(3)	Fe1–C3–N3	172.8(3)
Fe2–C5	1.922(9)	C4–Fe2–C5	81.4(5)	Fe2–C5	1.934(5)	C4–Fe2–C5	85.6(2)	Fe2–C5	1.934(3)	C4–Fe2–C5	84.3(1)
Fe2–C6	1.91(1)	C4–Fe2–C6	87.8(5)	Fe2–C6	1.932(6)	C4–Fe2–C6	82.3(2)	Fe2–C6	1.917(3)	C4–Fe2–C6	85.0(1)
Fe2–N14	2.003(7)	C5–Fe2–C6	89.0(4)	Fe2–N14	1.983(5)	C5–Fe2–C6	85.7(2)	Fe2–N14	2.011(3)	C5–Fe2–C6	88.3(1)
Fe2–N16	1.972(6)	C4–Fe2–N14	172.8(3)	Fe2–N16	2.008(5)	C4–Fe2–N14	92.8(2)	Fe2–N16	2.015(3)	C4–Fe2–N14	173.0(1)
Fe2–N18	1.984(6)	C4–Fe2–N16	93.9(3)	Fe2–N18	2.002(4)	C4–Fe2–N16	92.8(2)	Fe2–N18	2.014(3)	C4–Fe2–N16	95.7(1)
Ni1–N1	2.024(7)	N14–Fe2–N18	91.3(3)	Ni1–N1	2.034(5)	N14–Fe2–N18	90.5(2)	Ni1–N1	2.030(3)	N14–Fe2–N18	90.5(1)
Ni1–N4	2.045(7)	N16–Fe2–N18	87.6(2)	Ni1–N4	2.077(5)	N16–Fe2–N18	90.3(2)	Ni1–N4	2.079(3)	N16–Fe2–N18	89.0(1)
Ni1–N19	2.078(8)	Fe2–C4–N4	172.7(7)	Ni1–N19	2.084(5)	Fe2–C4–N4	173.2(5)	Ni1–N19	2.095(3)	Fe2–C4–N4	173.1(3)
Ni1–N20	2.082(8)	Fe2–C5–N5	174.5(8)	Ni1–N20	2.143(5)	Fe2–C5–N5	177.4(5)	Ni1–N20	2.084(3)	Fe2–C5–N5	178.2(3)
Ni1–N21	2.067(8)	Fe2–C6–N6	173(1)	Ni1–N21	2.131(5)	Fe2–C6–N6	173.6(5)	Ni1–N21	2.119(3)	Fe2–C6–N6	179.3(3)
Fe1···Ni1	5.090(8)	N1–Ni1–N19	89.0(3)	Fe1···Ni1	5.042(5)	N1–Ni1–N19	94.3(2)	Ni1–O1	2.145(2)	N1–Ni1–N19	99.2(1)
Fe1···Fe2	7.292(8)	N1–Ni1–N20	90.4(3)	Fe1···Fe2	7.361(8)	N1–Ni1–N20	95.8(2)	Fe1···Ni1	5.10(1)	N1–Ni1–N20	176.1(1)
		N1–Ni1–N21	174.3(3)			N1–Ni1–N21	97.8(2)	Fe1···Fe2	7.88(1)	N1–Ni1–N4	91.3(1)
		N1–Ni1–N22	94.7(3)			N1–Ni1–N22	177.6(2)			N1–Ni1–O1	88.6(1)
		N1–Ni1–N4	89.4(3)			N1–Ni1–N4	89.3(2)			O1–Ni1–N4	177.6(1)
		N19–Ni1–N20	77.7(3)			N19–Ni1–N20	94.4(2)			O1–Ni1–N20	88.0(1)
		N19–Ni1–N21	93.9(3)			N19–Ni1–N21	93.7(2)			O1–Ni1–N21	92.3(1)
		Ni1–N1–C1	174.3(7)			Ni1–N1–C1	165.9(5)			N19–Ni1–N20	82.8(1)
		Ni1–N4–C4	175.7(7)			Ni1–N4–C4	166.0(5)			Ni1–N1–C1	176.3(3)
										Ni1–N4–C4	167.6(3)

respectively (Figure S4, left). At 300 K, the χT value is 0.66 cm^3 K mol^{-1} and clearly indicates that **2** adopts an $S = {}^1/_2$ spin ground state (with $g = 2.65$), while **1** is diamagnetic, consistent with the presence of $Fe^{II}{}_{LS}$ centers. We note that large g factors are typically seen for this family of $[(Tp^R)Fe^{III}(CN)_3]$ building blocks, where Tp^R is a poly(pyrazolyl)borate, owing to the presence of degenerate spin ground states (^2E) and significant first-order orbital contributions to their spin ground states.[12,14,28–53,68–72] Consistent with this assumption, the χT product decreases towards a minimum of 0.54 cm^3 K mol^{-1} with decreasing temperature, and saturation magnetization data collected below 10 K confirms that **2** adopts an $S = {}^1/_2$ ground state, reaching a constant value of 1.1 μ_B at 1.8 K and $H_{dc} = 7$ T (Figure S4, right).

As judged from the magnetic data compounds **3**–**5** adopt $S = 2$ spin ground states owing to ferromagnetic exchange between orthogonal magnetic orbitals on the Ni^{II} ($S = 1$) and $Fe^{III}{}_{LS}$ ($S = {}^1/_2$) ions.[12,14,28–53,68–72,76–94] The room-temperature χT values for **3**–**5** [2.8, 2.7, and 2.6 cm^3 K mol^{-1}] are comparable and close to the one [2.6 cm^3 K mol^{-1}] expected for a 2:1 ratio of magnetically isolated $Fe^{III}{}_{LS}$ ($S = {}^1/_2$; $2.6 \le g \le 2.8$) and Ni^{II} ($S = 1$; $2.0 \le g \le 2.2$) spin centers (Figure 2 and Figures S5–S7). With decreasing temperature the χT products rapidly increase towards maximum values of 5.53, 5.22, and 4.23 cm^3 K mol^{-1} near ca. 10 K, confirming the onset of ferromagnetic interactions between the $Fe^{III}{}_{LS}$ and Ni^{II} ions in **3**–**5**, respectively. Reminiscent of other cyanide-bridged Fe^{III}/Ni^{II} complexes the χT products rapidly decrease below 10 K reaching minimum values of 3.21, 3.44, and 2.25 cm^3 K mol^{-1}, respectively, at 1.8 K.[12,14–46,70]

For simplicity the χT vs. T data for **3**–**5** were initially modelled using a single isotropic intracomplex magnetic exchange interaction, neglecting low-temperature data ($T < 5$ K) to avoid various issues associated with $\{Fe^{III}{}_2Ni^{II}\}$ anisotropy and/or weak intercomplex magnetic interactions. Using the following isotropic Heisenberg Hamiltonian [Equation (1)]:

$$H = -2J_1[S_1 \cdot (S_2 + S_3)] \quad (1)$$

where J_1 is the exchange interaction between the Fe^{III} and Ni^{II} sites and S_i are the spin operators for each metal center ($S_1 = 1$, Ni^{II}; $S_i = {}^1/_2$, $Fe^{III}{}_{LS}$ with $i = 2, 3$). Using a fitting procedure described by Song et al.,[39] J_1/k_B and g_{iso} are estimated to be: +11(1) K and 2.48(1), +9.1(1) K and 2.6(1), and +11.2(1) K and 2.41(5), for **3**–**5**, respectively (Figure 3, left; Figures S8 and S9). We note that g_{iso} falls within the typical range, while the J/k_B parameters deduced for **3** and **5** are somewhat higher than those encountered for **4** and other $\{Fe^{III}{}_2Ni^{II}\}$ complexes (Table S1).[12,32,35,40–46,70] MAGPACK[85,86] simulations of the χT vs. T data confirm that a respectable energy difference (ca. 22.4 K) between the ground ($S_T = 2$) and first excited ($S = 1$) state is present in **5** (Figure 3, bottom), and efforts to simulate the χT vs. T data using two different J_{Fe-Ni} and $g_{Fe}{}^{III}$ and $g_{Ni}{}^{II}$ terms and/or intermolecular exchange (via zJ'), led to overparameterization and physically unrealistic values for **3** and **4**.

The field dependence of the magnetization data collected between 1.8 and 10 K show that the magnetization approaches maximum values of 4.35, 4.52, and 4.76 μ_B at 1.8 K (for H_{dc} = 7 T) verifying that **3**–**5** adopt ferromagnetic $S_T = 2$ ground states (with $g_{iso} > 2$) (Table S2 and Figures S10–S12). Moreover, the reduced magnetization data (M vs. $H\,T^{-1}$) suggests that significant magnetic anisotropy is present in each complex as the M vs. $H\,T^{-1}$ curves are not superimposable over the temperature ranges investigated. Upon further inspection, the M vs. H data collected at 1.8 K for **5** also displays an inflection point, indicating that intercomplex antiferromagnetic interactions may be operative at low temperatures (Figure S13). Consistent with this assumption, application of increasing dc magnetic fields allows for an estimation of the intermolecular interactions relative to the Zeeman ones in **5** (Figure S13). Using this approach a crude estimation of the intermolecular interaction (zJ') by the $g\mu_B H^* S_T = 2zJ'S_T{}^2$ relationship leads to $zJ'/k_B = -0.28$ K.

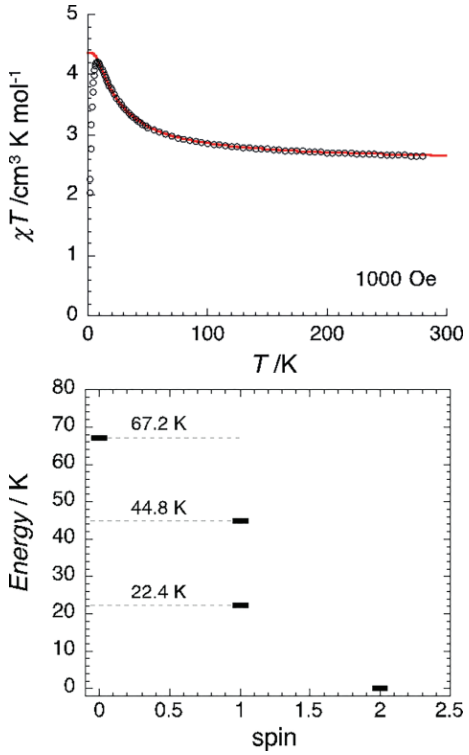

Figure 3. (top) Temperature dependence of the χT product of **5** collected between 1.8 and 300 K (H_{dc} = 1 kOe). Red line represents fitting of the data to an isotropic Heisenberg spin Hamiltonian [Equation (1)]. (bottom) Energy-level diagram for **5**.

In an effort to ascertain whether the magnetic anisotropy in **3**–**5** translates into sizeable SMM energy barriers we initiated a series of ac susceptibility measurements to investigate whether any of the complexes display slow magnetic-relaxation dynamics (Figure 4; Figures S14 and S15). Surprisingly, **3** and **4** do not display slow relaxation, while frequency-dependent dynamics are clearly seen for **5** above 10 kHz (for $H_{dc} = 0$ Oe), suggesting that rapid quantum tunnelling (QTM) of the magnetization occurs (Figure 4; Figures S14 and S15). Assuming that QTM is efficient in **5** we chose to apply a small dc magnetic field under the assumption that the QTM rate would decrease. As expected, application of a static dc magnetic field does decrease the characteristic frequency (Figure S15), but does not significantly slow

the relaxation rate at 1.85 K and up to $H_{dc} \approx 4000$ Oe. Given that many small SMMs generally undergo spin-lattice relaxation by non-Orbach processes our inability to fit the ac susceptibility data to an Arrhenius law suggests that thermally induced magnetic relaxation does not dominate the relaxation dynamics in **3**–**5** and is also consistent with the observation of rapid QTM in the trinuclear complexes.[77,87–102]

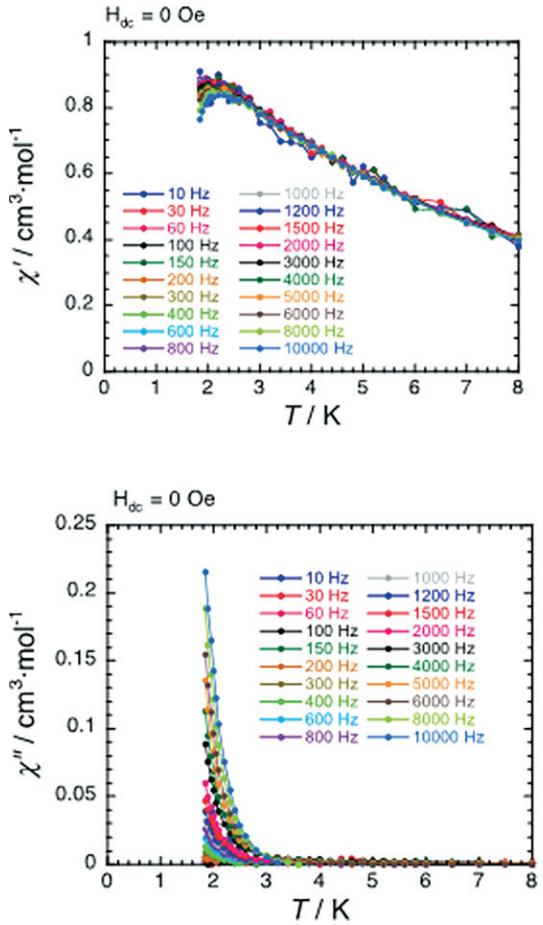

Figure 4. Temperature dependence of the in-phase (top) and out-of-phase (bottom) components of the ac susceptibility between 10 and 10000 Hz (H_{ac} = 3 Oe; H_{dc} = 0 Oe) for **5** below 8 K.

In $[(Tp^R)Fe^{III}_{LS}(CN)_3]^-$ complexes (Figure S16) significant magnetic anisotropy arising from first-order orbital contributions to their $S = {}^1/_2$ spin ground states are generally found. Under ideal C_{3v} symmetry the Fe^{III}_{LS} ions adopt $(z^2)^2(xz,yz)^3$ electronic configurations, which leads to doubly degenerate ^2E states, rather than triply degenerate $(xz,yz,xy)^5$ or $^2T_{2g}$ states, expected under O_h symmetry.[12,14,21,38–47,70–72] The relative energies of the metal-based orbitals are: $z^2 < (xz,yz) < (x^2 - y^2,xy)$,[103,104] which was previously confirmed by density-functional theory calculations of structurally related $[(Tp^*)Mn^{III}(CN)_3]^-$ anions. We note that C_{3v}-symmetric tricyanomanganate(III) ions adopt an isotropic $^3A_2$ state rather than a magnetically anisotropic $^3T_{2g}$ one seen for octahedral $[Mn^{III}_{LS}(CN)_6]^{3-}$.[12,14,21,38–47,70–72,112,113]

Density-functional theory calculations were performed at the B3LYP/DGDZVP level for the $[NEt_4][(Tp^R)Fe^{III}_{LS}(CN)_3]$ series (Figures S17–S22).[77,105] The data shows that ordering within the 3d manifold conforms to the following: $z^2 < (xz,yz) < (x^2 - y^2,xy)$, with smaller differences between the *xz* and *yz* orbitals (ca. 27–82 eV) for the trispyrazolylborates (Figures S17–S20). Interestingly the tetrapyrazolylborates display singly degenerate 3d orbitals (Figures S21 and S22). In all analogues extensive spin delocalization occurs by orbital mixing of the iron *xz* and *yz* orbitals with the cyanide π^* ones, with the greatest overlap seen for the electron-rich Tp^{*Me} analogue. Overall, the data qualitatively mirrors ligand-dependent trends seen in the spectroscopic data (vide infra).

In the $[NEt_4][(Tp^R)Fe^{III}(CN)_3]$ family of complexes the g_{iso} values deduced from magnetic data appear to qualitatively scale with the steric demand of the poly(pyrazolyl)borate (Tp^R) ligands (Table S2). We find that the magnitude of g_{iso} decreases from 2.92 to 2.35 as the C–Fe–C angle becomes more acute [from 87.7(1) to 88.2(1)°] for the Tp* to Tp^{*Bn} series, respectively (Figure S23). Interestingly, for less sterically demanding ligands (e.g. pzTp and Tp), slightly larger g_{iso} values are found for angles larger than ca. 88.5°, suggesting that metal–ligand bonding interactions play an important role in establishing single-ion anisotropy.

Comparing the electronic spectra (λ_{max}), electrochemical, and structural data collected for the tricyano complexes indicates that there are several likely relationships present for the $[NEt_4][(Tp^R)Fe^{III}(CN)_3]$ series (Figures S24–S26 and Table S1). For the (Tp^{*Me} → pzTp) series, the lowest-energy ligand-to-metal charge-transfer (LMCT) absorptions are found for those containing highly substituted and electron-rich ligands (e.g. Tp^{*Me}). These complexes also display the most negative Fe^{III}/Fe^{II} couples (Figure 5, top) and lowest energy ν_{CN} absorptions (in acetonitrile solution; Figures S24 and S25). Comparing λ_{max} energies to average cyanide C–Fe–C angles the highest energy LMCT absorptions are generally found for sterically less demanding and electron-poor ligands (e.g. Tp; Figures S26 and S27), which often have larger average C–Fe–C angles and the smallest mean plane Fe•••$[C_{CN}]_3$ distances in the series (Figure S27).

We also find that there may be a qualitative relationship linking structural distortions and magnetic anisotropy as reflected in the g_{iso} terms for the tricyanoferrates. The *g* terms are generally found to decrease with increasing C–Fe–C angle and distance of the Fe^{III} center from the mean plane containing the cyanide carbon atoms (Figure S23) for the Tp* → pzTp series. Additionally, the g_{iso} values also decrease with increasing λ_{max} and more positive $E_{1/2}$ values suggesting that orbital contributions to the spin ground state may be related to the extent of metal–ligand bonding interactions (Figure 5, top). However, comparing other structural features to the infrared and magnetic data do not readily provide additional insight.

Four general factors contribute to reductions in spin-orbit coupling. These are related to metal–ligand orbital mixing, availability of excited states, ligand spin-orbit coupling, and change in the nephelauxetic properties of the complex.[106–121] In the above mononuclear complexes we find that electron-deficient ones generally afford the highest-energy infrared ν_{CN} stretching and electronic LMCT (λ_{max}) absorptions, which is con-

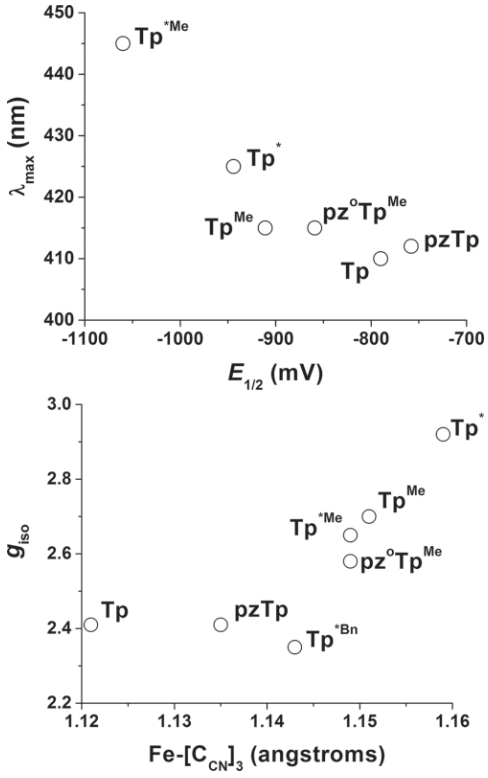

Figure 5. (top) Absorption maxima (λ_{max}) vs. $E_{1/2}$ of various $[NEt_4][(Tp^R)Fe^{III}(CN)_3]$ salts in MeCN solution. All potentials are referenced to the Fc/Fc^+ redox couple. (bottom) Landé g parameter vs. mean plane $Fe–[C_{CN}]_3$ distance for various $[NEt_4][(Tp^R)Fe^{III}(CN)_3]$ salts.

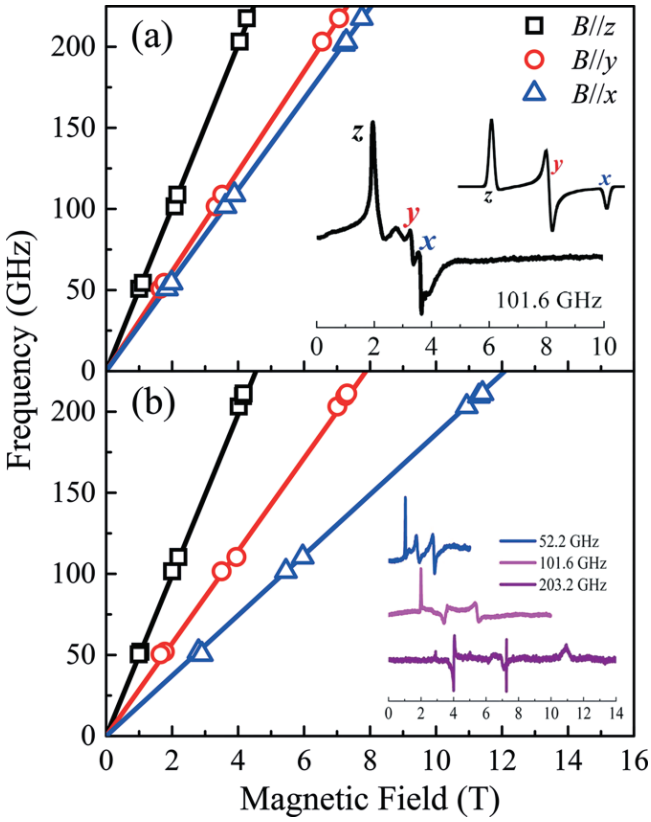

Figure 6. Frequency dependence of powder EPR peak positions for **2** (a) and **6** (b), collected between 50 and 218 GHz, at 5 and 10 K, respectively; the solid lines are simulations. The lower inset to (a) shows a representative derivative-mode (dI/dB, I = intensity) spectrum for **2**, while the upper inset depicts a simulation for a biaxial system, illustrating the lineshapes expected for the x, y and z components of the g-tensor; the corresponding features have been labeled in the lower inset. The inset to (b) shows representative dI/dB powder spectra for **6** at three different frequencies.

sistent with the most positive $Fe^{II/III}$ redox couples of the series (Figure 5, top; Table S1). These electron-deficient complexes also appear to have the smallest $Fe\cdots[C_{CN}]_3$ contacts and g_{iso} values suggesting that removal of electron density from the metal center leads to lower magnetic anisotropy (Figure 5, bottom).[127–140] This behavior is reminiscent of square-pyramidal {bis(imino)pyridine}$Co^{II}(NCS)_2$ complexes described by Murugesu, where increasing Co^{II} center distances from the basal mean $[N_4]$ plane lead to larger zero-field splitting arising from increasing orbital contributions to their $S = {}^3/_2$ spin ground states.[87]

Consistent with g_{iso} trends seen in the magnetic data, powder EPR spectroscopy verifies that **2** and structurally related $[NEt_4][(Tp^{*Me})Fe^{III}(CN)_3]\cdot 4H_2O$ (**6**) display dramatic differences in their single-ion magnetic anisotropy (Figure 6).[76,77] Frequency-dependent powder EPR data for **2** and **6** were collected between 50 and 218 GHz, at 5 and 10 K, respectively. The spectra display three resonance branches that intersect the frequency vs. field origin that are attributed to x (triangles), y (circles), and z (squares) intra-Kramers components of the ground-state spin doublet. Simulations of the frequency-dependent EPR data give anisotropic g-values of $g_z = 3.7$ and 3.5, $g_y = 2.2$ and 2.0, and $g_x = 1.92$ and 1.3, for **2** and **6**, respectively. These anisotropic values are consistent with significant first-order orbital contributions to their ^2E symmetry spin ground states (under C_{3v} symmetry).

Surprisingly, of the three trinuclear complexes, only **5** displayed slow magnetic relaxation in its ac susceptibility data. Consequently, we chose to further investigate its properties by high-field EPR spectroscopy. Previous oriented single-crystal investigations at multiple frequencies confirmed an easy-axis-type magnetic anisotropy in **5**,[76] with fits yielding the following spin Hamiltonian parameters: $S_T = 2$, $D = -2.09$ cm^{-1}, $E = 0.08$ cm^{-1}, $B_4^0 = -2.3 \times 10^{-3}$ cm^{-1}, $g_z = 2.4$, and $g_y = g_x = 1.95$. These values are comparable to those seen for other $\{Fe_2^{III}Ni^{II}\}$ complexes (Table S2).[12,28,32,76,77]

Over the past decade we investigated structure-property relationships relating to single-ion anisotropy tensor alignment, relative orientations of pseudo-C_3 rotation axes in $[(Tp^R)Fe^{III}(CN)_3]^-$ ions, intermolecular contacts, and relaxation dynamics in a variety of polynuclear magnetic complexes.[12,14,21–35,44,76] In many polynuclear $\{Fe^{III}{}_nNi^{II}{}_m\}$ clusters the orientation of the $Fe\cdots B$ vectors (C_3 axes) appear to serve as structural markers for $Fe^{III}{}_{LS}$ anisotropy tensor directionality. Interestingly, these axes also function as qualitative predictors for SMM energy barrier heights, where parallel orientations generally afford the highest experimental values [up to $\Delta_{eff}/k_B = 33$ K for an $\{Fe^{III}{}_4Ni^{II}{}_4\}$ complex].[12,31,32,34] In the trinuclear $\{Fe^{III}{}_2Ni^{II}\}$ series both bent and linear complexes (Table S2), with

Fe^{III}_{LS} sites related by crystallographic inversion, appear to afford the highest SMM energy barriers, while those of lower symmetry generally do not display slow dynamics above 1.8 K. For example, the linear and bent trinuclear $S = 2$ complexes, $\{[(Tp^{*Bn})Fe^{III}(CN)_3]_2[Ni^{II}(DMF)_4]\}\cdot 2DMF$[12,28] and $\{[(pzTp)Fe^{III}(CN)_3]_2[Ni^{II}(bpy)_2]\}\cdot 2H_2O$,[12,32] have similar exchange coupling constants (J_{iso}/k_B = 7.1 and 7.0 K) and SMM energy barriers (Δ_{eff}/k_B = 17 and 21 K) despite different spatial arrangements of their $[(Tp^R)Fe^{III}(CN)_3^-]$ fragments. In these complexes, their pseudo-C_3 axes (B1···Fe1) are related by crystallographic mirror and inversion symmetry, and their putative anisotropy tensors adopt ca. 180 and 71° orientations, respectively. In comparison, the lower-symmetry trinuclear analogues, $\{[(pzTp)Fe^{III}(CN)_3]_2[Ni^{II}(IM\text{-}2Py)_2]\}\cdot 2DMF\cdot H_2O\cdot {}^1/_2Et_2O$[12,45] and $\{[(pzTp)Fe^{III}(CN)_{32}][Ni^{II}(L)]\}\cdot {}^1/_2MeOH$,[12,32] each have significantly bent Fe(μ-CN)Ni units and are not SMMs. In complexes **3** and **4**, the Fe···B vectors are also unrelated by crystallographic symmetry, and the quasi-C_{3v} axes (e.g. B1···Fe1 and B2···Fe2) are rotated relative to one another (ca. 26.7 and 23.0°), while those in **5** (ca. 3.4°) are nearly colinear.

Under the assumption that the B···Fe axes are coincident with the Fe^{III}_{LS} single-ion anisotropy tensors, a comparatively larger SMM energy barrier is expected for **5**, while those for **3** and **4** should be considerably smaller. However, despite efficient ferromagnetic interactions [J/k_B = +11.2(1) K], a nearly parallel alignment of the putative single-ion magnetic anisotropy tensors, and a respectable energy separation between the ground and first excited state (ca. 22.4 K), we were surprised that only **5** displays SMM dynamics near 1.8 K. We propose that low symmetry and small spin ground states of the complexes likely lead to rhombic terms that encourage efficient QTM.

Conclusions

We have described how the magnetic properties of various structurally related tricyanoferrate(III) complexes change with ligand substitution. For the first time we show by high-field EPR studies that considerable *g* anisotropy is present in the $[NEt_4][(Tp^R)Fe^{III}(CN)_3]$ salts, particularly those where tetragonal distortions are more pronounced. We propose that ligand-induced steric distortions of the iron centers lead to the structure-dependent changes in the single-ion magnetic anisotropy. We also find for a family of trinuclear ferromagnetic $\{Fe^{III}_2Ni^{II}\}$ complexes that the magnetic properties may be tuned by intracluster ligand steric interactions that ultimately afford a means to tune the spatial orientations of single-ion anisotropy tensors.

Experimental Section

General Considerations: $NiCl_2\cdot 6H_2O$ (Acros), $Ni(ClO_4)_2\cdot 6H_2O$ (Acros), tris(2-aminoethyl)amine (tren; Acros), 2,2′-bipyridine (bpy; Acros), diethylenetriamine (DETA; Acros), *N*,*N*-dimethylformamide (Aldrich), 30 % H_2O_2 (Fisher), anhydrous $MgSO_4$ (Fisher), and deionized water were used as received. Solvents were distilled under dinitrogen from CaH_2 (acetonitrile, dichloromethane), sodium/benzophenone (diethyl ether) or Mg turnings (methanol, 2-propanol). $Fe(OAc)_2$,[73] KTp^{*Me},[54] and $[NEt_4]CN$[74] were prepared according to literature methods. Deionized water was used as received.

Physical Measurements: The IR spectra were recorded as Nujol mulls between KBr plates and as MeCN solutions with a Thermo-Electron Nicolet 6700 FTIR instrument in the 400–4000 cm^{-1} region. Thermogravimetric analysis data was collected with a TA Instruments Q500 instrument. UV/Vis spectra were collected as MeCN solutions with a Varian Cary spectrophotometer. Magnetic measurements on microcrystalline samples of **2**–**5** were performed with a Quantum Design MPMS-XL SQUID magnetometer. Alternating current (ac) susceptibility measurements were conducted using an oscillating ac field of 3 Oe. The magnetic data were corrected for the sample holder, and diamagnetic corrections were estimated using Pascal's constants.[122] Elemental analyses were performed by Robertson Microlit Laboratories. High-field powder EPR data were collected at the US National High Magnetic Field Laboratory Electron Magnetic Resonance facility using a transmission probe in which microwaves are propagated through cylindrical light-pipes. High-frequency microwaves were generated by a phase-locked Virginia Diodes solid-state source operating at 13 ± 1 GHz, followed by a chain of multipliers and amplifiers. High magnetic fields were provided by a 17 T superconducting magnet.[123]

$[NEt_4]_2[(Tp^{*Me})Fe^{II}(CN)_3]\cdot$MeCN (1): Dropwise addition of a DMF/MeCN (1:1, v/v; 40 mL) solution of KTp^{*Me} (2.40 g, 6.36 mmol) to a DMF solution (20 mL) of $Fe(OAc)_2$ (2.20 g, 12.6 mmol) over 30 min afforded a gray mixture, that was stirred at 50 °C for an additional 3 h. The residue was extracted with MeCN (2 × 20 mL), filtered, and added dropwise to a stirred MeCN (30 mL) solution of $[NEt_4]CN$ (2.98 g, 19.1 mmol). The resulting brown suspension was stirred for an additional 4 h and filtered to remove a brown precipitate. The filtrate was concentrated to ca. 20 mL, and Et_2O (90 mL) addition gave a red precipitate. The solid was isolated by suction filtration, washed with Et_2O (2 × 5 mL), and dried under vacuum for 2 min. Yield: 3.05 g (63.8 %). X-ray quality crystals were obtained by slow diffusion of Et_2O into a concentrated MeCN solution of **1**. The solid was immediately used in the preparation of **2**. IR (KBr/Nujol): $\tilde{\nu}$ = 3392 (m, br), 2954 (vs), 2924 (vs), 2854 (vs), 2498 (m), 2053 (s), 2041 (s), 2031 (s), 1654 (w), 1541 (m), 1458 (vs), 1377 (vs), 1354 (s), 1243 (s), 1184 (m), 1170 (m), 1092 (m), 1053 (w), 950 (w), 823 (m), 786 (m), 724 (w), 631 (w), 555 (w) cm^{-1}.

$[NEt_4][(Tp^{*Me})Fe^{III}(CN)_3]\cdot H_2O$ (2): Dropwise addition of aqueous 30 % H_2O_2 (20 mL) to a CH_2Cl_2/*i*PrOH (4:1, v/v; 50 mL) solution of **1** (3.05 g, 4.06 mmol) over 30 min afforded a red mixture, that was stirred for an additional 3 h. The aqueous phase was decanted and the organic phase dried with anhydrous $MgSO_4$ to give a red-brown solution. The mixture was filtered, concentrated under vacuum (to ca. 10 mL), and Et_2O (60 mL) addition gave a red powder. Yield: 1.75 g (69.3 %). Red crystals were obtained by slow concentration of an MeOH/H_2O (2:1, v/v) solution of **2**. $C_{29}H_{50}BFeN_{10}O$ (621.4): calcd. C 56.05, H 8.11, N 22.54; found C 56.05, H 7.90, N 22.46. IR (KBr/Nujol): $\tilde{\nu}$ = 3501 (s), 3442 (s), 2923 (vs), 2855 (vs), 2545 (s), 2124 (s), 2116 (s), 1668 (w), 1639 (m), 1560 (m), 1514 (s), 1456 (vs), 1382 (vs), 1365 (vs), 1308 (w), 1295 (vs), 1245 (w), 1172 (m), 1145 (w), 887 (w), 870 (s), 834 (s), 783 (s), 736 (s), 723 (m), 692 (w), 671 (w), 628 (w), 565 (w), 544 (w), 532 (w), 498 (m), 470 (w), 401 (s) cm^{-1}.

$\{[(Tp^{*Me})Fe(CN)_3]_2[Ni(bpy)_2]\}\cdot 3H_2O\cdot 4$MeOH (3): Addition of MeOH (10 mL) to a solid mixture of $NiCl_2\cdot 6H_2O$ (24.2 mg, 0.102 mmol) and bpy (32.5 mg, 0.208 mmol) initially afforded a light pink solution that was stirred for 1 h. The mixture was quickly added to an MeOH (10 mL) solution of **2** (125 mg, 0.201 mmol) to give a dark red solution. The mixture was stirred for 2 min, filtered, and left at room temperature for 7 d. The dark red crystals were collected by suction filtration, washed with H_2O (3 mL) and 95 % EtOH (3 mL), and dried under vacuum at room temperature for 2 min. Yield: 74.8 mg

(50.7 %). $C_{65}H_{90}B_2Fe_2N_{22}NiO_6$ (**3**-MeOH, 1467.6): calcd. C 53.19, H 6.19, N 20.99; found C 50.17, H 5.93, N 20.85. IR (KBr/Nujol): $\tilde{\nu}$ = 3530 (m), 3358 (s, br.), 3125 (s), 3125 (s), 3069 (s), 2943 (vs), 2942 (vs), 2904 (vs), 2857 (vs), 2533 (m), 2159 (m), 2121 (m), 1636 (w), 1605 (m), 1598 (m), 1576 (w), 1567 (m), 1544 (s), 1508 (m), 1491 (m), 1450 (vs), 1416 (s), 1375 (vs), 1313 (w), 1249 (w), 1204 (s), 1161 (m), 1061 (s), 1024 (s), 984 (w), 868 (w), 816 (w), 785 (m), 774 (m), 738 (m), 693 (w), 651 (m) cm^{-1}.

{[(Tp*^{Me})Fe^{III}(CN)$_3$]$_2$[Ni^{II}(tren)]}·2H$_2$O·3MeOH (4): Dropwise addition of methanolic (5 mL) tren (18.5 mg, 0.126 mmol) to a solution of $NiCl_2·6H_2O$ (23.5 mg, 0.100 mmol) in MeOH (5 mL) afforded a pale blue solution that was stirred for 1 h. The mixture was quickly added to an MeOH (10 mL) solution of **2** (123 mg, 0.198 mmol), which rapidly became dark red in color; the mixture was stirred for an additional 2 min, filtered, and left at room temperature for 7 d. The dark red crystals were isolated by suction filtration, washed with H_2O (2 × 3 mL) and 95 % EtOH (3 mL), and dried under vacuum for 2 min. Yield: 73.6 mg (58.7 %). $C_{49}H_{88}B_2Fe_2N_{22}NiO_4$ (**4**-H_2O, 1241.4): calcd. C 48.12, H 7.02, N 24.34; found C 48.12, H 6.24, N 24.14. IR (KBr/Nujol): $\tilde{\nu}$ = 3354 (s, br.), 2924 (vs), 2853 (vs), 2536 (m), 2153 (m), 2119 (m), 1635 (w), 1609 (w), 1563 (w), 1520 (m), 1456 (vs), 1377 (vs), 1243 (s), 1175 (m), 1101 (m), 1054 (m), 1025 (m), 995 (m), 977 (m), 874 (w), 889 (m), 737 (m), 690 (w), 667 (w), 628 (w), 543 (w), 473 (w), 403 (m) cm^{-1}.

{[(Tp*^{Me})Fe^{III}(CN)$_3$]$_2$[Ni^{II}(DETA)(OH$_2$)]}·6H$_2$O·MeCN (5):[76] Dropwise addition of DETA (10.5 mg, 0.102 mmol) in MeCN (2 mL) to an MeCN (3 mL) solution of $Ni(ClO_4)_2·6H_2O$ (37.3 mg, 0.102 mmol) afforded a purple solution that was stirred for 1 h. The solution was added to an MeCN/H_2O (1:1, v/v; 5 mL) solution of **2** (123 mg, 0.198 mmol) to produce a dark red solution. The mixture was magnetically stirred for 2 min, filtered, and left at room temperature for an additional 7 d. The dark red crystals were isolated by suction filtration, washed with H_2O (5 mL), MeCN (5 mL), and dried under vacuum at room temperature for 2 min. Yield: 72.0 mg (59.5 %). $C_{46}H_{85}B_2Fe_2N_{21}NiO_7$ (**5**-MeCN, 1236.3): calcd. C 45.20, H 7.02, N 24.05; found C 44.92, H 6.64, N 23.85. IR (Nujol): $\tilde{\nu}$ = 3378 (s, br.), 2923 (vs), 2854 (vs), 2529 (m), 2154 (m), 2122 (m), 1635 (w), 1609 (w), 1562 (w), 1457 (vs), 1377 (vs), 1366 (vs), 1233 (vs), 1173 (m), 1146 (vs), 1101 (vs), 1023 (s), 968 (vs), 952 (w), 889 (s), 873 (w), 833 (m), 795 (vw), 777 (vw), 735 (m), 722 (m), 689 (m), 668 (m), 626 (vw), 544 (w), 510 (vw), 475 (vw), 415 (m), 406 (s), 403 (m), 401 (w) cm^{-1}.

Structure Determinations and Refinements: X-ray structural data for **1**–**5** were collected at 100(2) K with a Bruker APEX-II CCD diffractometer. Crystals were mounted in Paratone-N oil on glass fibers, and the structures were solved by direct methods (SHELXS97)[124,125] and completed by difference Fourier methods (SHELXL97).[125] Refinement was performed against F^2 by weighted full-matrix least squares (SHELXL97),[125] and empirical absorption corrections (SADABS)[125] were applied. Hydrogen atoms were found in difference maps and subsequently placed at calculated positions using suitable riding models with isotropic displacement parameters derived from their carrier atoms. Non-hydrogen atoms were refined with anisotropic displacement parameters and atomic scattering factors were taken from the International Tables for Crystallography, vol. C.[126] Crystal data and selected geometrical parameters appear in Tables S1 and S2. CCDC 1455904 (for **1**), 768189 (for **2**), 1455906 (for **3**), 1455907 (for **4**), and 1455908 (for **5**) contain the supplementary crystallographic data for this paper. These data can be obtained free of charge from The Cambridge Crystallographic Data Centre.

Supporting Information (see footnote on the first page of this article): Additional magnetic and spectroscopic data.

Acknowledgments

S. M. H. gratefully acknowledges the National Science Foundation (CHE-0939987, X-ray upgrade; CHE-0914935, CAREER; CHE-1214063), the Missouri Research Board, the American Chemical Society Project SEED, and the University of Missouri – St. Louis (College of Arts and Sciences Research Award) for financial support. R. C. thanks the Centre National de la Recherche Scientifique (CNRS), the University of Bordeaux, the Conseil Régional d'Aquitaine, GIS Advanced Materials in Aquitaine (COMET Project) and the Agence Nationale de la Recherche (ANR) (NT09_469563, AC-MAGnets project) for financial support. Work performed at the National High Magnetic Field Laboratory is supported by the National Science Foundation (DMR-1157490) and by the State of Florida. S. H. acknowledges the support of the National Science Foundation (DMR-1309463). C. C. B. thanks the NHMFL Shuler Fellowship program.

Keywords: Single-molecule magnets · Cyanides · Clusters · Ferromagnetic compounds · Pyrazolylborate

[1] M. N. Leuenberger, D. Loss, *Nature* **2001**, *410*, 789.
[2] A. Caneschi, D. Gatteschi, R. Sessoli, A. L. Barra, L. C. Brunel, M. Guillot, *J. Am. Chem. Soc.* **1991**, *113*, 5873.
[3] A. L. Barra, A. Caneschi, A. Cornia, F. Fabrizi de Biani, D. Gatteschi, C. Sangregorio, R. Sessoli, L. Sorace, *J. Am. Chem. Soc.* **1999**, *121*, 5302.
[4] R. Sessoli, D. Gatteschi, A. Caneschi, M. A. Novak, *Nature* **1993**, *365*, 141.
[5] W. Wernsdorfer, N. Aliaga-Alcalde, G. Christou, *Science* **2003**, *302*, 1015.
[6] D. Ruiz, Z. Sun, B. Albela, K. Folting, J. Ribas, G. Christou, D. N. Hendrickson, *Angew. Chem. Int. Ed.* **1998**, *37*, 300; *Angew. Chem.* **1998**, *110*, 315.
[7] R. Sessoli, D. Gatteschi, *Angew. Chem. Int. Ed.* **2003**, *42*, 268; *Angew. Chem.* **2003**, *115*, 278, and references therein.
[8] D. Gatteschi, R. Sessoli, J. Villain, *Molecular Nanomagnets*, Oxford University Press, New York, **2006**, and references therein.
[9] C. J. Milios, A. Vinslava, W. Wernsdorfer, S. Moggach, S. Parsons, S. P. Perlepes, G. Christou, E. K. Brechin, *J. Am. Chem. Soc.* **2007**, *129*, 2754.
[10] L. M. C. Beltran, J. R. Long, *Acc. Chem. Res.* **2005**, *38*, 325.
[11] X. Y. Wang, C. Avendaño, K. R. Dunbar, *Chem. Soc. Rev.* **2011**, *40*, 3213, and references therein.
[12] P. J. Ferko, S. M. Holmes, *Curr. Inorg. Chem.* **2013**, *3*, 172, and references therein.
[13] R. Sessoli, M.-E. Boulon, A. Caneschi, M. Mannini, L. Poggini, F. Wilhelm, A. Rogalev, *Nature Phys.* **2015**, *11*, 67.
[14] K. Park, S. M. Holmes, *Phys. Rev. B* **2006**, *74*, 224440.
[15] S. Wang, X. H. Ding, J.-L. Zuo, X.-Z. You, W. Huang, *Coord. Chem. Rev.* **2011**, *255*, 1713, and references therein.
[16] S. Wang, J.-L. Zuo, H.-C. Zhou, H.-J. Choi, Y. Ke, J. R. Long, X.-Z. You, *Angew. Chem. Int. Ed.* **2004**, *43*, 5940; *Angew. Chem.* **2004**, *116*, 6066.
[17] J. J. Sokol, A. G. Hee, J. R. Long, *J. Am. Chem. Soc.* **2002**, *124*, 7656.
[18] C. P. Berlinguette, D. Vaughn, C. Canada-Vilalta, J. R. Gálan-Mascarós, K. R. Dunbar, *Angew. Chem. Int. Ed.* **2003**, *42*, 1523; *Angew. Chem.* **2003**, *115*, 1561.
[19] Y. Song, P. Zhang, X.-M. Ren, X.-F. Shen, Y.-Z. Li, X.-Z. You, *J. Am. Chem. Soc.* **2005**, *127*, 3708.
[20] C.-F. Wang, J.-L. Zuo, B. M. Bartlett, Y. Song, J. R. Long, X.-Z. You, *J. Am. Chem. Soc.* **2006**, *128*, 7162.
[21] D. F. Li, S. Parkin, G. B. Wang, G. T. Yee, A. V. Prosvirin, S. M. Holmes, *Inorg. Chem.* **2005**, *44*, 4903.
[22] E. J. Schelter, F. Karadas, C. Avendaño, A. V. Prosvirin, W. Wernsdorfer, K. R. Dunbar, *J. Am. Chem. Soc.* **2007**, *129*, 8139.
[23] D. E. Freedman, D. M. Jenkins, A. Iavarone, J. R. Long, *J. Am. Chem. Soc.* **2008**, *130*, 2884.
[24] Y.-Z. Zhang, B.-W. Wang, O. Sato, S. Gao, *Chem. Commun.* **2010**, *46*, 6959.
[25] K. R. Dunbar, E. J. Schelter, A. V. Palii, S. M. Ostrovsky, V. Y. Mirovitskii, J. M. Hudson, M. A. Omary, S. I. Klokishner, B. S. Tsukerblat, *J. Phys. Chem. A* **2003**, *107*, 11102.

[26] C. P. Berlinguette, D. Vaughn, C. Cañada-Vilalta, J. R. Galán-Mascarós, K. R. Dunbar, *Angew. Chem. Int. Ed.* **2003**, *42*, 1523; *Angew. Chem.* **2003**, *115*, 1561.
[27] A. V. Palii, S. M. Ostrovsky, S. I. Klokishner, B. S. Tsukerblat, C. P. Berlinguette, K. R. Dunbar, J. R. Galán-Mascarós, *J. Am. Chem. Soc.* **2004**, *126*, 16860.
[28] Y.-Z. Zhang, U. P. Mallik, N. P. Rath, R. Clérac, S. M. Holmes, *Inorg. Chem.* **2011**, *50*, 10537.
[29] D.-F. Li, S. Parkin, R. Clérac, S. M. Holmes, *Inorg. Chem.* **2006**, *45*, 7569.
[30] D.-F. Li, S. Parkin, G. B. Wang, G. T. Yee, S. M. Holmes, *Inorg. Chem.* **2005**, *44*, 1951.
[31] D.-F. Li, S. Parkin, G. B. Wang, G. T. Yee, R. Clérac, W. Wernsdorfer, S. M. Holmes, *J. Am. Chem. Soc.* **2006**, *128*, 4214.
[32] D.-F. Li, R. Clérac, S. Parkin, G.-B. Wang, G. T. Yee, S. M. Holmes, *Inorg. Chem.* **2006**, *45*, 5251.
[33] D.-F. Li, R. Clérac, G. Wang, G. T. Yee, S. M. Holmes, *Eur. J. Inorg. Chem.* **2007**, 1341.
[34] Y.-Z. Zhang, U. P. Mallik, N. P. Rath, G. T. Yee, R. Clérac, S. M. Holmes, *Chem. Commun.* **2010**, *46*, 4953.
[35] Y.-Z. Zhang, U. P. Mallik, R. Clérac, N. P. Rath, S. M. Holmes, *Chem. Commun.* **2011**, *47*, 7194.
[36] L. Jiang, H. J. Choi, X.-L. Feng, T. B. Lu, J. R. Long, *Inorg. Chem.* **2007**, *46*, 2181.
[37] C.-F. Wang, W. Liu, Y. Song, X.-H. Zhou, J.-L. Zuo, X.-Z. You, *Eur. J. Inorg. Chem.* **2008**, 717.
[38] D.-Y. Wu, Y. J. Zhang, W. Huang, O. Sato, *Dalton Trans.* **2010**, *39*, 5500.
[39] S. Wang, J.-L. Zuo, H.-C. Zhou, Y. Song, X.-Z. You, *Inorg. Chim. Acta* **2005**, *358*, 2101.
[40] C.-F. Wang, Z.-G. Gu, X.-M. Lu, J.-L. Zuo, X.-Z. You, *Inorg. Chem.* **2008**, *47*, 7957.
[41] J.-Z. Gu, L. Jiang, M.-Y. Tan, T.-B. Lu, *J. Mol. Struct.* **2008**, *890*, 24.
[42] W. Liu, C.-F. Wang, Y.-Z. Li, J.-L. Zuo, X.-Z. You, *Inorg. Chem.* **2006**, *45*, 10058.
[43] S. Wang, J.-L. Zuo, H.-C. Zhou, Y. Song, S. Gao, X.-Z. You, *Eur. J. Inorg. Chem.* **2004**, 3681.
[44] Z.-G. Gu, Q.-F. Yang, X.-H. Zhou, J.-L. Zuo, X.-Z. You, *Inorg. Chem.* **2007**, *46*, 3236.
[45] Y.-Z. Zhang, D.-F. Li, R. Clérac, S. M. Holmes, *Polyhedron* **2013**, *60*, 110.
[46] L. M. Toma, R. Lescouëzec, J. Pasán, C. Ruiz-Pérez, J. Vaissermann, J. Cano, R. Carrasco, W. Wernsdorfer, F. Lloret, M. Julve, *J. Am. Chem. Soc.* **2006**, *128*, 4842.
[47] D.-P. Zhang, L.-F. Zhang, Y.-T. Chen, H.-L. Wang, Z.-H. Ni, W. Wernsdorfer, J.-Z. Jiang, *Chem. Commun.* **2010**, *46*, 3550.
[48] T. D. Harris, M. V. Bennett, R. Clérac, J. R. Long, *J. Am. Chem. Soc.* **2010**, *132*, 3980.
[49] X. Feng, T. D. Harris, J. R. Long, *Chem. Sci.* **2011**, *2*, 1688.
[50] K. Mitsumoto, E. Oshiro, H. Nishikawa, T. Shiga, Y. Yamamura, K. Saito, H. Oshio, *Chem. Eur. J.* **2011**, *17*, 9612.
[51] S. Wang, J.-L. Zuo, S. Gao, Y. Song, H.-C. Zhou, Y.-Z. Zhang, X.-Z. You, *J. Am. Chem. Soc.* **2004**, *126*, 8900.
[52] H.-R. Wen, C.-F. Wang, Y. Song, S. Gao, J.-L. Zuo, X.-Z. You, *Inorg. Chem.* **2006**, *45*, 8942.
[53] C.-F. Wang, D.-P. Li, X. Chen, X.-M. Li, Y.-Z. Li, J.-L. Zuo, X.-Z. You, *Chem. Commun.* **2009**, *45*, 6940.
[54] S. Trofimenko, *Scorpionates – The Coordination Chemistry of Polypyrazolylborate Ligands*, Imperial College Press, London, **1999**, and references therein.
[55] D.-F. Li, R. Clérac, O. Roubeau, E. Harté, C. Mathonière, R. Le Bris, S. M. Holmes, *J. Am. Chem. Soc.* **2008**, *130*, 252.
[56] Y.-Z. Zhang, D.-F. Li, R. Clérac, M. Kalisz, C. Mathonière, S. M. Holmes, *Angew. Chem. Int. Ed.* **2010**, *49*, 3752; *Angew. Chem.* **2010**, *122*, 3840.
[57] N. Hoshino, Y. Sekine, M. Nihei, H. Oshio, *Chem. Commun.* **2010**, *46*, 6117.
[58] K. Mitsumoto, M. Ui, M. Nihei, H. Nishikawa, H. Oshio, *CrystEngComm* **2010**, *12*, 2697.
[59] T. Liu, Y. Zhang, S. Kanegawa, O. Sato, *Angew. Chem. Int. Ed.* **2010**, *49*, 8645; *Angew. Chem.* **2010**, *122*, 8827.
[60] T. Liu, Y. Zhang, S. Kanegawa, O. Sato, *J. Am. Chem. Soc.* **2010**, *132*, 8250.
[61] J. Mercurol, Y.-L. Li, E. Pardo, O. Risset, M. Seuleiman, H. Rousselière, R. Lescouëzec, M. Julve, *Chem. Commun.* **2010**, *46*, 8995.
[62] D. Siretanu, D.-F. Li, L. Buisson, D. M. Bassani, S. M. Holmes, C. Mathonière, R. Clérac, *Chem. Eur. J.* **2011**, *17*, 11704.
[63] M. Nihei, Y. Sekine, N. Suganami, K. Nakazawa, A. Nakao, H. Nakao, Y. Murakami, H. Oshio, *J. Am. Chem. Soc.* **2011**, *133*, 3592.
[64] T. Liu, D. P. Dong, S. Kanegawa, S. Kang, O. Sato, Y. Shiota, K. Yoshizawa, S. Hayami, S. Wu, C. He, C.-Y. Duan, *Angew. Chem. Int. Ed.* **2012**, *51*, 4367; *Angew. Chem.* **2012**, *124*, 4443.
[65] A. Mondal, Y. Li, M. Seuleiman, M. Julve, L. Toupet, M. Buron-Le Cointe, R. Lescouëzec, *J. Am. Chem. Soc.* **2013**, *135*, 1653.
[66] Y.-Z. Zhang, P. Ferko, D. Siretanu, R. Ababei, N. P. Rath, M. J. Shaw, R. Clérac, C. Mathonière, S. M. Holmes, *J. Am. Chem. Soc.* **2014**, *136*, 16854.
[67] E. S. Koumousi, I.-R. Jeon, Q. Gao, P. Dechambenoit, D. N. Woodruff, P. Merzeau, L. Buisson, X. Jia, D.-F. Li, F. Volatron, F. C. Mathonière, R. Clérac, *J. Am. Chem. Soc.* **2014**, *136*, 15461.
[68] M. Nihei, M. Ui, M. Yokota, L.-Q. Han, A. Maeda, H. Kishida, H. Okamoto, H. Oshio, *Angew. Chem. Int. Ed.* **2005**, *44*, 6484; *Angew. Chem.* **2005**, *117*, 6642.
[69] R. Herchel, R. Boca, M. Gembicky, J. Kozísek, F. Renz, *Inorg. Chem.* **2004**, *43*, 4103.
[70] I. Boldog, F. J. Munoz-Lara, A. B. Gaspar, M. C. Munoz, M. Seredyuk, J. A. Real, *Inorg. Chem.* **2009**, *48*, 3710.
[71] A. Panja, P. Guionneau, I.-R. Jeon, S. M. Holmes, R. Clérac, C. Mathoniere, *Inorg. Chem.* **2012**, *51*, 12350.
[72] S. Wang, J.-L. Zuo, H.-C. Zhou, Y. Song, X.-Z. You, *Inorg. Chim. Acta* **2005**, *358*, 2101.
[73] S. Kikichi, Y. Sasakura, M. Yoshizawa, Y. Ohzu, Y. Moro-oka, M. Akita, *Bull. Chem. Soc. Jpn.* **2002**, *75*, 1255.
[74] a) S. Andreades, E. Zahnow, *J. Am. Chem. Soc.* **1969**, *91*, 4181; b) S. M. Holmes, *Molecule-Based Magnets Constructed from Hexacyanometalates*, Ph. D. thesis, University of Illinois at Urbana-Champaign, Urbana, IL, **1999**.
[75] K. Nakamoto, *Infrared and Raman Spectra of Inorganic and Coordination Compounds*, part B, 5th ed., Wiley, New York, **1997**, pp. 54–58, 105–116.
[76] C. C. Beedle, Y.-Z. Zhang, S. M. Holmes, S. Hill, *Polyhedron* **2013**, *59*, 48.
[77] See the Supporting Information.
[78] O. Kahn, P. Prins, J. Reedijk, J. S. Thompson, *Inorg. Chem.* **1987**, *26*, 3557.
[79] H. Hiraga, H. Miyasaka, R. Clérac, M. Fourmigué, M. Yamashita, *Inorg. Chem.* **2009**, *48*, 2887.
[80] W. R. Entley, G. S. Girolami, *Science* **1995**, *268*, 397.
[81] S. Ferlay, T. Mallah, R. Ouahès, P. Veillet, M. Verdaguer, *Nature* **1995**, *378*, 701.
[82] S. M. Holmes, G. S. Girolami, *J. Am. Chem. Soc.* **1999**, *121*, 5593.
[83] M. Verdaguer, G. S. Girolami, *Magnetoscience: Molecules to Materials*, vol. V (Eds.: J. S. Miller, M. Drillon), Wiley, Weinheim, Germany, and references therein.
[84] J. Goodenough, *Magnetism and the Chemical Bond*, Wiley, New York, **1963**.
[85] J. J. Borrás-Almenar, J. M. Clemente-Juan, E. Coronado, B. S. Tsukerblat, *Inorg. Chem.* **1999**, *38*, 6081.
[86] J. J. Borrás-Almenar, J. M. Clemente-Juan, E. Coronado, B. S. Tsukerblat, *J. Comput. Chem.* **2001**, *22*, 985.
[87] T. Jurca, A. Farghal, P.-H. Lin, I. Korobkov, M. Murugesu, D. S. Richeson, *J. Am. Chem. Soc.* **2011**, *133*, 15814.
[88] G. A. Craig, M. Murrie, *Chem. Soc. Rev.* **2015**, *44*, 2135.
[89] S. Gómez-Coca, D. Aravena, R. Morales, E. Ruiz, *Coord. Chem. Rev.* **2015**, *289–290*, 379.
[90] M. Atanasov, D. Aravena, E. Suturina, E. Bill, D. Maganas, F. Neese, *Coord. Chem. Rev.* **2015**, *289–290*, 177.
[91] D. N. Woodruff, R. E. P. Winpenny, R. A. Layfield, *Chem. Rev.* **2013**, *113*, 5110.
[92] V. V. Novikov, A. A. Pavlov, Y. V. Nelyubina, M.-E. Boulon, O. A. Varatskii, Y. Z. Voloshin, R. E. P. Winpenny, *J. Am. Chem. Soc.* **2015**, *137*, 9792.
[93] S. Gómez-Coca, A. Urtizberea, E. Cremedes, P. J. Alonso, A. Camón, E. Ruiz, F. Luis, *Nat. Commun.* **2014**, *5*, 1.
[94] R. Boča, J. Miklovič, J. Titiš, *Inorg. Chem.* **2014**, *53*, 2367.
[95] M. R. Saber, K. R. Dunbar, *Chem. Commun.* **2014**, *50*, 12266.
[96] J. M. Zadrozny, J. Liu, J. Piro, N. A. Piro, C. J. Chang, S. Hill, J. R. Long, *Chem. Commun.* **2012**, *48*, 3927.
[97] J. M. Zadrozny, M. Atansov, A. Bryan, C. Y. Lin, B. D. Rekken, P. P. Power, J. R. Long, *Chem. Sci.* **2013**, *4*, 125.

[98] D. E. Freedman, W. H. Harman, T. D. Harris, G. J. Long, C. J. Chang, J. R. Long, *J. Am. Chem. Soc.* **2008**, *132*, 1224.
[99] R. C. Poulten, M. J. Page, A. G. Algarra, J. J. Le Roy, I. Lopez, E. Carter, A. Llobet, S. A. Macgregor, M. F. Mahon, D. M. Murphy, M. Murugesu, M. K. Whittlesey, *J. Am. Chem. Soc.* **2013**, *135*, 13640.
[100] I. Nemec, R. Herchel, I. Svoboda, R. Boča, Z. Trávníček, *Dalton Trans.* **2015**, *44*, 9551.
[101] K. E. R. Marriott, L. Bhaskaran, C. Wilson, M. Merdarde, S. T. Ochsenbein, S. Hill, M. Murrie, *Chem. Sci.* **2015**, *6*, 6823.
[102] K. S. Pedersen, J. Dreiser, H. Weihe, R. Sibille, H. V. Johannesen, M. A. SØrensen, B. E. Nielsen, M. Sigrist, H. Mutka, S. Rols, J. Bendix, *Inorg. Chem.* **2015**, *54*, 7600.
[103] M. Tang, D. Li, U. P. Mallik, J. R. Withers, S. Brauer, M. R. Rhodes, R. Clérac, G. T. Yee, M.-W. Whangbo, S. M. Holmes, *Inorg. Chem.* **2010**, *49*, 4753.
[104] M. Tang, D. Li, U. P. Mallik, Y.-Z. Zhang, R. Clérac, G. T. Yee, M.-H. Whangbo, A. Mungalimane, S. M. Holmes, *Inorg. Chem.* **2011**, *50*, 5153.
[105] M. J. Frisch, G. W. Trucks, H. B. Schlegel, G. E. Scuseria, M. A. Robb, J. R. Cheeseman, G. Scalmani, V. Barone, B. Mennucci, G. A. Petersson, H. Nakatsuji, M. Caricato, X. Li, H. P. Hratchian, A. F. Izmaylov, J. Bloino, G. Zheng, J. L. Sonnenberg, M. Hada, M. Ehara, K. Toyota, R. Fukuda, J. Hasegawa, M. Ishida, T. Nakajima, Y. Honda, O. Kitao, H. Nakai, T. Vreven, J. A. Montgomery Jr., J. E. Peralta, F. Ogliaro, M. Bearpark, J. J. Heyd, E. Brothers, K. N. Kudin, V. N. Staroverov, R. Kobayashi, J. Normand, K. Raghavachari, A. Rendell, J. C. Burant, S. S. Iyengar, J. Tomasi, M. Cossi, N. Rega, J. M. Millam, M. Klene, J. E. Knox, J. B. Cross, V. Bakken, C. Adamo, J. Jaramillo, R. Gomperts, R. E. Stratmann, O. Yazyev, A. J. Austin, R. Cammi, C. Pomelli, J. W. Ochterski, R. L. Martin, K. Morokuma, V. G. Zakrzewski, G. A. Voth, P. Salvador, J. J. Dannenberg, S. Dapprich, A. D. Daniels, Ö. Farkas, J. B. Foresman, J. V. Ortiz, J. Cioslowski, D. J. Fox, *Gaussian 09*, revision E.01, Gaussian, Inc., Wallingford, CT, **2009**.
[106] A. J. Stone, *Proc. R. Soc. (London)* **1954**, *A226*, 96.
[107] A. H. Maki, B. R. McGarvey, *J. Chem. Phys.* **1958**, *29*, 31.
[108] A. J. Stone, *Proc. R. Soc. (London)* **1963**, *A271*, 424.
[109] D. Kivelson, R. Neimann, *J. Chem. Phys.* **1961**, *35*, 149.
[110] B. R. McGarvey, *Transition Met. Chem.* **1966**, *3*, 89.
[111] C. P. Keijzers, E. DeBoer, *J. Chem. Phys.* **1972**, *57*, 1277.
[112] D. W. Smith, *J. Chem. Soc. A* **1970**, 3108.
[113] C. K. Jørgensen, *Orbitals in Atoms and Molecules*, Academic Press, London, **1962**.
[114] C. K. Jørgensen, *Adv. Chem. Phys.* **1963**, *5*, 33.
[115] C. K. Jørgensen, *Struct. Bonding (Berlin)* **1966**, *1*, 3.
[116] C. K. Jørgensen, *Struct. Bonding (Berlin)* **1969**, *6*, 94.
[117] R. L. Belford, M. Karplus, *J. Chem. Phys.* **1959**, *31*, 394.
[118] J. S. Griffith, *The Theory of Transition Metal Ions*, Cambridge University Press, Cambridge, **1964**.
[119] C. J. Ballhausen, *Introduction to Ligand Field Theory*, McGraw Hill, New York, **1962**.
[120] F. Neese, E. I. Solomon, *Inorg. Chem.* **1998**, *37*, 6568.
[121] F. E. Mabbs, D. J. Machin, *Magnetism and Transition Metal Complexes*, Chapman and Hall, London, **1973**.
[122] E. A. Boudreaux, L. N. Mulay, *Theory and Applications of Molecular Paramagnetism*, Wiley, **1976**.
[123] A. K. Hassan, L. A. Pardi, J. Krzystek, A. Sienkiewicz, P. Goy, M. Rohrer, L. C. Brunel, *J. Magn. Reson.* **2000**, *142*, 300.
[124] G. M. Sheldrick, *SHELX-97, Programs for Crystal Structure Solution and Refinement*, University of Göttingen, Germany, **1997**.
[125] G. M. Sheldrick, *SADABS, An Empirical Absorption Correction Program*, Bruker Analytical X-ray Systems, Madison, WI, **1996**.
[126] *International Tables for Crystallography*, vol. C, Kluwer Academic Publishers, Dordrecht, Netherlands, **1992**.

Received: February 26, 2016
Published Online: May 13, 2016

